Synthesis, Characterization, and Photoelectrochemical Catalytic Studies of a Water-Stable Zinc-Based Metal–Organic Framework

Muhammad Altaf,*[a] Manzar Sohail,[a] Muhammad Mansha,[a, b] Naseer Iqbal,[a] Muhammad Sher,[a] Atif Fazal,[c] Nisar Ullah,[a, b] and Anvarhusein A. Isab[b]

Metal–organic frameworks (MOFs) are class of porous materials that can be assembled in a modular manner by using different metal ions and organic linkers. Owing to their tunable structural properties, these materials are found to be useful for gas storage and separation technologies, as well as for catalytic applications. A cost-effective zinc-based MOF ([Zn(bpcda)(bdc)]$_n$) is prepared by using N,N'-bis(pyridin-4-ylmethylene)cyclohexane-1,4-diamine [N,N'-bis(pyridin-4-ylmethylene)cyclohexane-1,4-diamine] and benzenedicarboxylic acid (bdc) linkers. This new material exhibits remarkable photoelectrochemical (PEC) catalytic activity in water splitting for the evolution of oxygen. Notably, this non-noble metal-based MOF, without requiring immobilization on other supports or containing metal particles, produced a highest photocurrent density of 31 µA cm^{-2} at 0.9 V, with appreciable stability and negligible photocorrosion. Advantageously for the oxygen evolution process, no external reagents or sacrificial agents are required in the aqueous electrolyte solution.

The development of suitable methods to obtain and utilize energy from renewable resources is an essential task for mankind, both now and in the future.[1] At present, fossil fuels are the main source to meet the energy demands of humans at an affordable cost.[2] However, limited reserves and the estimated exhaustion of fossil fuels, along with the detrimental usage of these fuels to environment, have spurred interest to look for alternative energy sources.[3] In this regard, solar energy and water are considered to be the most sustainable and renewable resources. However, the utilization of these resources remains challenging.[4] A key step in harnessing solar energy is its conversion into useful chemical energy. Thus, efficient H$_2$ generation by solar water splitting constitutes a promising way to utilize and store energy.[5] Throughout the last decade, intensive research efforts have been devoted to developing processes for H$_2$ generation by water splitting[6] Among these processes, photoelectrochemical (PEC) approaches have emerged as a promising technology for achieving sustainable generation of H$_2$ fuel from water.[7] For this challenging process, the development of suitable semiconductor materials with tunable band gaps is highly important.[8] For this purpose, various mixed-metal-composite semiconductors are suitable because their band gaps can be easily tuned to generate electrons in the conduction band and holes in the valence band upon solar illumination.[9] To attain sufficient activity, the fast recombination of electrons and holes generated must be prevented to allow sufficient time to migrate to the surface of the catalysts and participate in redox reactions for H$_2$ generation from water.[10] Although significant efforts have been made to develop photocatalysts for sunlight-assisted water splitting, newly developed materials remain highly desired. In this regard, metal–organic frameworks (MOFs) are a suitable choice, owing to their diverse structural modes.

The chemistry of MOFs has evolved significantly over the last few years. MOFs adopt highly ordered structures with significantly high surface areas. These materials, built from metal ions and organic linkers, can produce desirable structures that can incorporate catalytic centers and light-harvesting components within a single compound.[11] In general, most MOFs are insulators and are used only as a high-surface-area support for metal-based semiconducting nanostructured catalytic centers. Some MOFs are used as cocatalysts alongside dyes or composite semiconductors to promote kinetic processes and diminish electron/hole recombination.[12] In recent studies, MOFs have been applied as a cocatalyst supported on TiO$_2$ for light harvesting and can significantly enhance the visible-light water-splitting activity of TiO$_2$ photocatalysts.[13] Moreover, MOFs can also be used directly as photo- or photoelectrocatalysts.[12, 14] Notably, MOFs act as heterogeneous and homogeneous catalysts as well as semiconducting materials based on metals and organic linker moieties. The band gaps of MOFs can be easily modulated by introducing different functional groups on the linkers. Thus, MOFs are rapidly finding their place in a diverse range of fields, including electronics (termed as MOFtronics), lithium-ion batteries, supercapacitors, and dye-sensitized solar cells.[15] However, the design of MOFs for PEC applications

[a] Dr. M. Altaf, Dr. M. Sohail, Dr. M. Mansha, Dr. N. Iqbal, Dr. M. Sher, Prof. N. Ullah
Centre of Research Excellence in Nanotechnology (CENT)
King Fahd University of Petroleum and Minerals
Dhahran 31261 (Saudi Arabia)
E-mail: muhammadaltaf@kfupm.edu.sa

[b] Dr. M. Mansha, Prof. N. Ullah, Prof. A. A. Isab
Department of Chemistry
King Fahd University of Petroleum and Minerals
Dhahran 31261 (Saudi Arabia)

[c] Dr. A. Fazal
Center of Research Excellence in Petroleum Refining and Petrochemicals (CoRE-PRP)
King Fahd University of Petroleum and Minerals
Dhahran 31261 (Saudi Arabia)

⧉ Supporting Information for this article can be found under: https://doi.org/10.1002/cssc.201702122.

remains a challenge and hence few reports are known on their direct utilization in PEC systems.[14]

To split water, a semiconducting photocatalyst should have a valence band with a more positive potential than the H_2O/O_2 couple (1.23 eV) and a conduction band with a more negative potential than the H_2O/H_2 couple (0.00 eV). In MOFs, the height of the valence band can be manipulated by introducing different functionalities on the organic linker and the conduction-band level depends on the coordination mode of the metal center. In general, solar light reaching the Earth consists of 47% visible light and only 2% UV light. Thus, an efficient solar-light-sensitized semiconducting MOF should be responsive within the visible-light range (400–700 nm) and should have an efficient valence and conduction band separation to allow enough time for charge transfer from the linker to the cluster. A band gap smaller than 3.0 eV is required for an active visible-light photocatalyst.

The development of MOFs provides an opportunity to decorate hierarchically ordered light-harvesting catalytic centers within the same molecule, enabling the direct utilization of sunlight to obtain useful chemicals in the presence of a suitable feedstock. In this regard, MOFs and MOF-supported photocatalysts have been studied for the H_2 evolution half reaction.[14, 16] However, very few works are known for the more challenging and energy-demanding oxygen-evolution half reaction. This is mainly due to the instability and diminished catalytic activity in reaction media required for the oxygen evolution reaction. The need for strong oxidizing agents, complementary sacrificial agents, and control of pH value makes it tedious to use MOFs for these applications. Previously, nanocomposites were developed for water oxidation by doping Ir- and Mn-based photocatalysts in relatively stable MOFs (UiO-67 and Zr-MOF) for Ce^{IV}-driven water oxidation. However, in these cases, catalytic activity was diminished and long-term stability also remained an issue.[17] In addition, electrocatalytic water oxidation with cobalt-based MOFs was reported, but the authors inferred that catalytic activity might be due to the cobalt-oxide nanoparticles formed through the decomposition of the Co-MOF rather than intrinsic activity of the MOFs themselves.[18] Encapsulation of TiO_2 nanoparticles was reported within titanium-derived MIL-125, MIL-125-NH_2, and MIL-125-$(NH_2)_{1,2}$ MOFs. These TiO_2/Ti-MOF hybrid nanocomposites were mounted on fluorine-doped tin oxide (FTO) and used as photoanodes. To further enhance the PEC activity, gold nanoparticles were decorated on the MOF network. The resulting Au@TiO_2/MOF nanocomposite produced a PEC current of 30 μA cm^{-2}, which is comparable to many reported semiconducting nanostructures.[13] Nevertheless, the development of earth-abundant metal-based MOFs is highly important for cost-effective photoelectrochemical water oxidation. In this regard, we report herein a new [Zn(bpcda)(bdc)]$_n$ MOF [bpcda = N,N'-bis(pyridin-4-ylmethylene)cyclohexane-1,4-diamine, bdc = benzenedicarboxylic acid] and its utilization as a photoanode in a PEC cell for water oxidation. To our knowledge, we are reporting for the first time a MOF that is used directly for the oxygen evolution reaction that does not require any oxidizing reagents in the electrolyte solution. Advantageously, our MOF material

acts as both photoelectrocatalyst and oxidant for water splitting to produce oxygen.

We began the preparation of [Zn(bpcda)(bdc)]$_n$ MOF (hereafter denoted Zn-MOF) by using a solvothermal synthesis method. This new MOF was characterized by elemental analysis, NMR and FTIR spectroscopy, and single-crystal X-ray diffraction (for details, see the Supporting Information). The crystal structure of Zn-MOF is shown in Figure 1. This MOF crystallizes
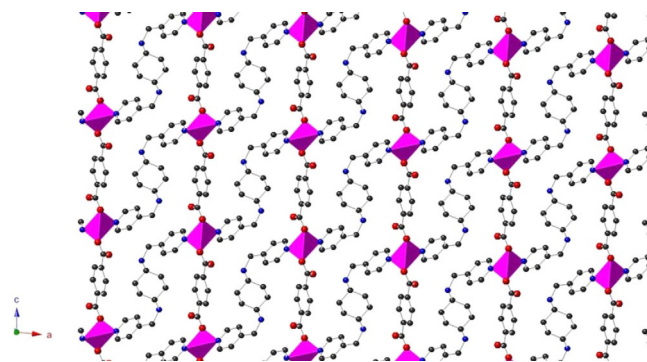

Figure 1. Polyhedral view of the 3D framework along the *c* axis. Hydrogen atoms are omitted for clarity.

in a monoclinic crystal system with space group *C*2/*c*. The X-ray structure analysis reveals that the asymmetric unit of the MOF consists of one Zn^{II} cation and one unit of each bpcda and bdc linkers. Single-crystal X-ray diffraction indicates that the Zn^{II} compound is in a three-dimensional interpenetrating diamondoid framework. The Zn^{II} center adopts a distorted tetrahedral geometry and is coordinated with two N atoms of two independent bpcda linkers and two O atoms of two independent bdc linkers (Figure S1 in the Supporting Information). The Zn—N and Zn—O bond lengths are 1.959(1) and 2.048(1) Å, respectively. The minimum and maximum bond angles involving the Zn^{II} ion are 100.77(8) and 125.37(5)° respectively. The average bond angle value is 107.67°, which shows deviation from the ideal angle of 109.47° for a perfect tetrahedron. Houser and co-workers reported a simple geometric index for four-coordinate metal system ($\tau4 = 360° - (\alpha + \beta)/141°$, where α and β are largest angles in the four-coordinate metal system).[19] The distortion from an ideal tetrahedron for Zn atom is 0.93, as indicated by the $\tau4$ value.

The X-ray structure shows that each bdc dianion connects to adjacent Zn^{II} centers in a bridging *trans*-monodentate mode, resulting in zigzag chains that are further extended by the bpcda linkers to form a three-dimensional diamondoid framework (Figures S2 and S3). The Zn^{II} compound has a dia-like topology by considering the Zn^{II} centers as 4-connected nodes and bpcda and bdc as linkers.[20] Each Zn^{II} center node is connected to four neighbors, forming an adamantane-like cage, which is a characteristic building block for a diamondoid framework. The Zn···Zn separations along Zn···bdc···Zn and Zn···bpcda···Zn are 11.034 and 16.989 Å, respectively. Owing to the large Zn···Zn separations, large cavities are formed within each network. To minimize the big voids in the framework, five

independent equivalent networks interpenetrate each other for effective filling of the voids. The interpenetration of equivalent frameworks results in a three-dimensional architecture.[21]

The optical absorption of $[Zn(bpcda)(bdc)]_n$ was investigated by using UV/Vis diffuse-reflectance spectroscopy (DRS; Figure 2). Although a maximum absorption was observed at
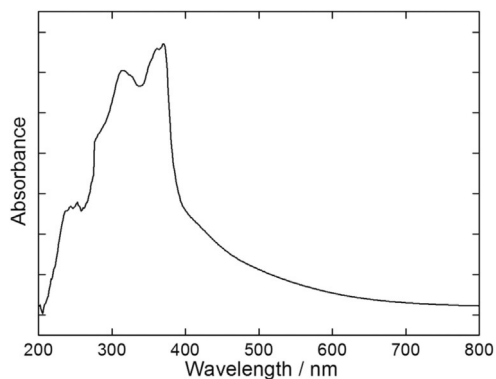

Figure 2. DRS absorption spectra of $[Zn(bpcda)(bdc)]_n$.

370 nm (3.3 eV), a long absorption tail was extended up to 600 nm. In addition, another absorption peak was observed at 313 nm (3.9 eV). Therefore, Zn-MOF was not only capable of absorbing wide range of sunlight radiation but also showed multiple HOMO/LUMO levels within the same compound. These multiple absorption bands can be attributed to the presence of two different ligands and metal centers. The presence of multiple band gaps in the same structure provides efficient separation between electron and hole pairs without addition of any dopant and is responsible for the enhanced PEC activity of the Zn-MOF.

After detailed characterization of the material, we demonstrated its activity for photoelectrochemical water splitting. Photoelectrochemical studies of Zn-MOF were carried out by using FTO conducting glass substrates. Initially, FTO substrates were washed with acetone (10 min) and deionized water (10 min), respectively, with continuous ultrasonication. The next step involved slurry formation of the Zn-MOF samples with ethanol. Once a reasonably thick slurry was prepared, the Zn-MOF sample was drop-coated over the pretreated FTO glass substrates. To generate a smooth film, the drop-coated Zn-MOF/FTO samples were annealed at 80 °C for 2 h to evaporate solvent and harden the layers over the FTO substrate, so that it could withstand the PEC measurements. PEC measurements were carried out by a standard three-electrode system in 0.5 M Na_2SO_4 (pH 7.0) solution, with Pt wire as auxiliary electrode, the Zn-MOF-coated FTO substrate served as photoanode, and Ag/AgCl (sat. KCl) as reference electrode. All PEC experiments were executed with a Metrohm Autolab Potentiostat (PGSTAT302N) instrument. An Oriel sol 3A class AAA solar simulator-Newport Instrument (power = 100 mW cm^{-2} (1 Sun), IEC/JIS/ASTM-certified 450 W Xenon lamp, AM 1.5G Filter, UV cutoff filter, and 2×2 in^2 (1 in = 2.54 mm) aperture for output beam) was used as the irradiation source. All PEC experimental

data obtained were discussed according to the standard Ag/AgCl (sat. KCl) electrode. In chronoamperometric measurements, the PEC cell was exposed to illumination source (1 sun) in an on/off fashion with regular time intervals, to investigate the photoresponse generated by $[Zn(bpcda)(bdc)]_n$. Bare FTO showed almost negligible photoresponse at the same applied potential range. These characteristics elucidate solar water splitting and O_2 evolution reaction of $[Zn(bpcda)(bdc)]_n$ and its potential applications in PEC processes. The generated photocurrent in PEC studies is attributed to the better electron mobility and minimal electron–hole recombination offered by $[Zn(bpcda)(bdc)]_n$. To our knowledge, a photocurrent response for the oxygen evolution reaction in water splitting has not been reported to date with a MOF as the sole material, without being supported on other heterogeneous material or containing metal particles. Furthermore, no additional oxidant, sacrificial agent, or pH control was required, thus providing a favorable environment for enhanced stability of the Zn-MOF. Figure 3 shows the chronoamperometric performance of the
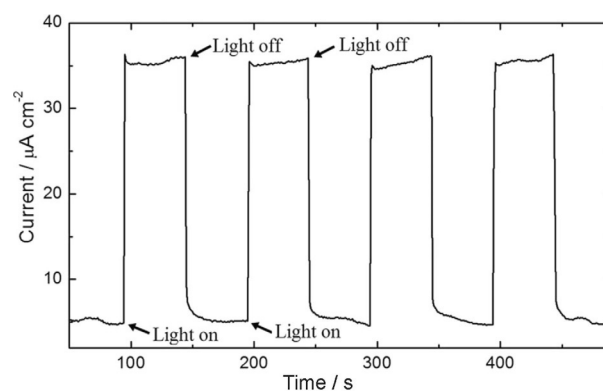

Figure 3. Chronoamperometry curve with 50 s on/off solar light for $[Zn(bpcda)(bdc)]_n$/FTO photoanode at 0.9 V applied potential (Ag/AgCl/sat. KCl).

$[Zn(bpcda)(bdc)]_n$/FTO photoanode at 0.9 V (vs. Ag/AgCl) as a function of time under simulated sunlight illumination. Once the current response was stable, the light was cut off at regular intervals. When the surface of the $[Zn(bpcda)(bdc)]_n$/FTO electrode was illuminated, significant anodic current was produced for O_2 generation. When the light was cut off, the photocurrent density instantaneously became negligible. The amount of generated current was approximately 16 µA cm^{-2}. The photocurrent density spikes (J_p peaks) indicated the significant stability of the $[Zn(bpcda)(bdc)]_n$-coated FTO upon exposure to 1 sun irradiation for several hours. Furthermore, in successive PEC measurements, we observed shifting of the J_p–t photocurrents to its normal baseline under dark (no illumination), which exhibited reversible responses. These observations also established that photocurrent generation from Zn-MOF was exclusively due to solar-driven water splitting.

Figure 4 shows linear sweep voltammetry (LSV) curves of $[Zn(bpcda)(bdc)]_n$/FTO phononode (Ag/AgCl/sat. KCl) under 1 sun-simulated solar light. LSV was carried out with solar light

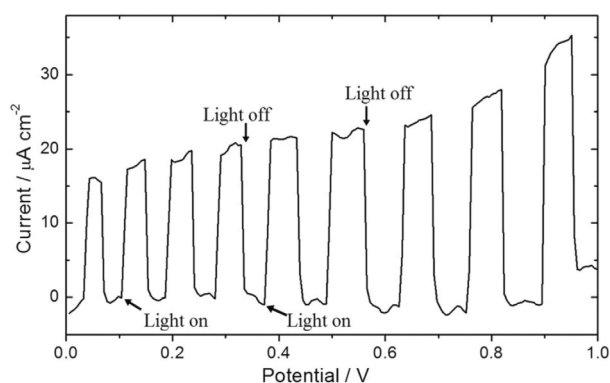**Figure 4.** Linear sweep voltammetry of [Zn(bpcda)(bdc)]$_n$ coated on FTO glass under simulated solar light chopped at regular intervals (scan rate = 10 mV s^{-1}).

Figure 5. Chronoamperometery stability curves of Zn-MOF/FTO photoanode at 0 V (Ag/AgCl/sat. KCl).

chopped at regular intervals and applied potential scanned from 0.0 to 1.0 V at 10 mV s^{-1}. Figure 4 shows the LSV curve after subtracting the dark current. The overall current density at 1.0 V exceeds 80 µA cm^{-2}. After subtracting the dark current density at 0 V (Ag/AgCl/sat. KCl), a pure photocurrent density of approximately 15 µA cm^{-2} was observed at 0 V, which increased linearly with increasing bias voltage. A maximum photocurrent density exceeding 31 µA cm^{-2} was observed at 0.9 V. This current response is comparable to or better than many recently reported metal nanocomposite-based semiconductors (Table 1).[22–28]

Table 1. Comparison of the photoresponse of [Zn(bpcda)(bdc)]$_n$ for water splitting with those of some recently reported semiconducting nanocomposite materials.

Nanocomposite photoanode	Measurement voltage [V]	Photocurrent [µA cm^{-2}]	Ref.
WO$_3$—BiO$_4$	0	2	[22]
CuS QDs:TiO$_2$[a]	1	15	[23]
ZnO:Cl/Zn$_x$TiO$_y$/TiO$_2$	1	0.4	[24]
PbTiO$_3$	1.02	15	[25]
PbTiO$_3$·PtO nanodots	1.02	60	[25]
TiO$_2$·g-C$_3$N$_4$[b] (2 h prep. time)	0.6	20	[26]
TiO$_2$·g-C$_3$N$_4$[b] (4 h prep. time)	0.6	30	[26]
TiO$_2$·g-C$_3$N$_4$[b] (6 h prep. time)	0.6	60	[26]
hierarchical WO$_3$	0	0.3	[27]
hierarchical Bi$_2$O$_3$/WO$_3$	0	0.9	[27]
WO$_3$/BiVO$_4$ nanoflakes	0	10	[28]
[Zn(bpcda)(bdc)]$_n$ MOF	0–0.9	15–31	this work

[a] QDs = quantum dots. [b] g-C$_3$N$_4$ = graphitic carbon nitride.

To demonstrate the practical utility of any photoelectrocatalysts, stability is the key factor Therefore, we tested the stability of [Zn(bpcda)(bdc)]$_n$/FTO photoanode in the dark and under 1 sun light illumination (Figure 5). The [Zn(bpcda)(bdc)]$_n$/FTO anode exhibited high stability over 1500 s. The dark current was very stable, whereas a noisy photocurrent was observed, owing to O$_2$ evolution and accumulation of O$_2$ bubbles at the surface for both electrodes.[29] A small decrease in photocurrent response was observed over time, which could be recov-
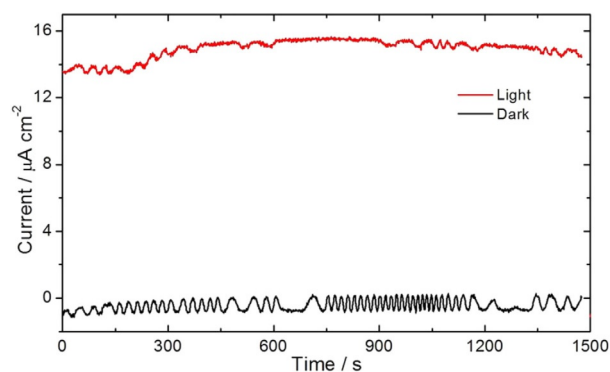
ered when the solution was stirred to remove O$_2$ bubbles from the electrode surface. Thus, the [Zn(bpcda)(bdc)]$_n$ photoanode acted as an efficient water-oxidation catalyst in neutral sodium sulfate solution. Overall, a reproducible response was observed during the entire experimental time (exceeding 12 h) with a single [Zn(bpcda)(bdc)]$_n$/FTO electrode. The most interesting features observed in the chronoamperometric experiments were that there was negligible photocorrosion and very good photoresponse stability. Consequently, this [Zn(bpcda)(bdc)]$_n$ material is a promising candidate for anodic water splitting applications.

In conclusion, we have reported the synthesis of a novel zinc-based metal–organic framework. The X-ray structure analysis displayed that [Zn(bpcda)(bdc)]$_n$ is a three-dimensional (3D) framework that contains 1,4-benzenedicarboxylic acid (1,4-bdc) and bpcda = N,N'-bis(pyridin-4-ylmethylene)cyclohexane-1,4-diamine (bpcda) linkers. In this structure, each bdc anion connects with the metal center in bridging mode, resulting in 1D chains that are linked by the bipyridyl bpcda linker to form a 3D diamondoid framework. The application of this metal–organic framework (MOF) was demonstrated for photoelectrochemical (PEC) water splitting. PEC measurements with this MOF displayed photocurrent densities in the microampere range with negligible photocorrosion and appreciable stability. Linear sweep voltammetry (LSV) and chronoamperometry studies showed oxygen evolution as a result of solar-driven water splitting. This implies that MOFs can be tuned for direct PEC water splitting and other electrochemical applications without supporting nanostructures.

Experimental Section

A mixture of Zn(NO$_3$)$_2$·6H$_2$O (0.297 g, 1.0 mmol), N,N'-bis(pyridin-4-ylmethylene)cyclohexane-1,4-diamine (bpcda) (0.297 g, 1.0 mmol), H$_2$bdc (0.172 g, 1.0 mmol), and a mixture of DMF and H$_2$O (10 mL, 3:1 v/v) were mixed and placed in glass vial. The vial was then loosely capped and heated at 105 °C for three days. Colorless block-shaped crystals were obtained after the vial was cooled to room temperature, washed with DMF (10 mL×3), and dried in air. CCDC 1452209 contains the supplementary crystallographic data for this paper. These data are provided free of charge by The Cambridge Crystallographic Data Centre.

[1] H. B. Wu, B. Y. Xia, L. Yu, X.-Y. Yu, X. W. Lou, *Nat. Commun.* **2015**, *6*, 6512.

[2] J.-R. Li, Y. Ma, M. C. McCarthy, J. Sculley, J. Yu, H.-K. Jeong, P. B. Balbuena, H.-C. Zhou, *Coord. Chem. Rev.* **2011**, *255*, 1791 – 1823.

[3] a) I. S. Nashawi, A. Malallah, M. Al-Bisharah, *Energy Fuels* **2010**, *24*, 1788 – 1800; b) N. Armaroli, V. Balzani, *Angew. Chem. Int. Ed.* **2007**, *46*, 52 – 66; *Angew. Chem.* **2007**, *119*, 52 – 67; c) M. Fontecave, *Angew. Chem. Int. Ed.* **2015**, *54*, 6946 – 6947; *Angew. Chem.* **2015**, *127*, 7050 – 7051.

[4] a) T. R. Cook, D. K. Dogutan, S. Y. Reece, Y. Surendranath, T. S. Teets, D. G. Nocera, *Chem. Rev.* **2010**, *110*, 6474 – 6502; b) M. G. Walter, E. L. Warren, J. R. McKone, S. W. Boettcher, Q. Mi, E. A. Santori, N. S. Lewis, *Chem. Rev.* **2010**, *110*, 6446 – 6473.

[5] Q. Liu, J. Tian, W. Cui, P. Jiang, N. Cheng, A. M. Asiri, X. Sun, *Angew. Chem.* **2014**, *126*, 6828 – 6832.

[6] S. Rajaambal, K. Sivaranjani, C. S. Gopinath, *J. Chem. Sci.* **2015**, *127*, 33 – 47.

[7] X. Yang, A.-Y. Lu, Y. Zhu, M. N. Hedhili, S. Min, K.-W. Huang, Y. Han, L.-J. Li, *Nano Energy* **2015**, *15*, 634 – 641.

[8] W. S. Choi, M. F. Chisholm, D. J. Singh, T. Choi, G. E. Jellison, Jr., H. N. Lee, *Nat. Commun.* **2012**, *3*, 689.

[9] V. Subramanian, E. Wolf, P. V. Kamat, *J. Phys. Chem. B* **2001**, *105*, 11439 – 11446.

[10] a) M. Reza Gholipour, C.-T. Dinh, F. Beland, T.-O. Do, *Nanoscale* **2015**, *7*, 8187 – 8208; b) T. Zhang, W. Lin, *Chem. Soc. Rev.* **2014**, *43*, 5982 – 5993.

[11] a) C. Gomes Silva, I. Luz, F. X. Llabrés i Xamena, A. Corma, H. García, *Chem. Eur. J.* **2010**, *16*, 11133 – 11138; b) D. Sheberla, J. C. Bachman, J. S. Elias, C.-J. Sun, Y. Shao-Horn, M. Dincă, *Nat. Mater.* **2016**, *16*, 220.

[12] S. Wang, X. Wang, *Small* **2015**, *11*, 3097 – 3112.

[13] L. Zhang, P. Cui, H. Yang, J. Chen, F. Xiao, Y. Guo, Y. Liu, W. Zhang, F. Huo, B. Liu, *Adv. Sci.* **2016**, *3*, 1500243.

[14] K. Meyer, M. Ranocchiari, J. A. van Bokhoven, *Energy Environ. Sci.* **2015**, *8*, 1923 – 1937.

[15] Z. Xie, W. Xu, X. Cui, Y. Wang, *ChemSusChem* **2017**, *10*, 1645 – 1663.

[16] M. Xu, L. Han, Y. Han, Y. Yu, J. Zhai, S. Dong, *J. Mater. Chem. A* **2015**, *3*, 21471 – 21477.

[17] R. E. Hansen, S. Das, *Energy Environ. Sci.* **2014**, *7*, 317 – 322.

[18] a) Y. Gong, H.-F. Shi, P.-G. Jiang, W. Hua, J.-H. Lin, *Cryst. Growth Des.* **2014**, *14*, 649 – 657; b) Y. Gong, Z. Hao, J. Meng, H. Shi, P. Jiang, M. Zhang, J. Lin, *ChemPlusChem* **2014**, *79*, 266 – 277.

[19] L. Yang, D. R. Powell, R. P. Houser, *Dalton Trans.* **2007**, 955 – 964.

[20] a) A. C. Wibowo, M. D. Smith, H.-C. zur Loye, *CrystEngComm* **2011**, *13*, 426 – 429; b) Z. Xu, L. L. Han, G. L. Zhuang, J. Bai, D. Sun, *Inorg. Chem.* **2015**, *54*, 4737 – 4743; c) Z. Wang, X.-Y. Li, L.-W. Liu, S.-Q. Yu, Z.-Y. Feng, C.-H. Tung, D. Sun, *Chem. Eur. J.* **2016**, *22*, 6830 – 6836.

[21] M. Altaf, M. Mansha, M. Sohail, A. A. Isab, N. Ullah, S. A. Khan, M. Sher, H. Stoeckli-Evans, *New J. Chem.* **2017**, *41*, 2980 – 2986.

[22] N. Iqbal, I. Khan, Z. H. A. Yamani, A. Qurashi, *Solar Energy* **2017**, *144*, 604 – 611.

[23] J. Du, M. Yang, F. Zhang, X. Cheng, H. Wu, H. Qin, Q. Jian, X. Lin, K. Li, D. J. Kang, *Ceram. Int.* **2018**, *44*, 3099 – 3106.

[24] F. Jiandong, Z. Reza, F. Cristian, S. Alexey, F. Cristina, I. Maria, A. Teresa, M. L. Antonio, A. Jordi, M. Joan Ramón, C. Andreu, *J. Phys. D* **2012**, *45*, 415301.

[25] C. W. Ahn, P. H. Borse, J. H. Kim, J. Y. Kim, J. S. Jang, C.-R. Cho, J.-H. Yoon, B.-s. Lee, J.-S. Bae, H. G. Kim, J. S. Lee, *Appl. Catal. B* **2018**, *224*, 804 – 809.

[26] X. Fan, T. Wang, B. Gao, H. Gong, H. Xue, H. Guo, L. Song, W. Xia, X. Huang, J. He, *Langmuir* **2016**, *32*, 13322 – 13332.

[27] I. Khan, A. Abdalla, A. Qurashi, *Int. J. Hydrogen Energy* **2017**, *42*, 3431 – 3439.

[28] A. A. M. Ibrahim, I. Khan, N. Iqbal, A. Qurashi, *Int. J. Hydrogen Energy* **2017**, *42*, 3423 – 3430.

[29] K. Zeng, D. Zhang, *Prog. Energy Combust. Sci.* **2010**, *36*, 307 – 326.